ADVANCED FUNCTIONAL MATERIALS
www.afm-journal.de

www.MaterialsViews.com

A Highly Efficient, Blue-Phosphorescent Device Based on a Wide-Bandgap Host/FIrpic: Rational Design of the Carbazole and Phosphine Oxide Moieties on Tetraphenylsilane

He Liu, Gang Cheng, Dehua Hu, Fangzhong Shen, Ying Lv, Guannan Sun, Bing Yang, Ping Lu, and Yuguang Ma**

A new series of wide-bandgap materials, 4-dipenylphosphine oxide-4′-9H-carbazol-9-yl-tetraphenylsilane (CSPO), 4-diphenylphosphine oxide-4′,4″-di(9H-carbazol-9-yl)-tetraphenylsilane (pDCSPO), 4-diphenylphosphine oxide -4′-[3-(9H-carbazol-9-yl)-carbazole-9-yl]-tetraphenylsilane (DCSPO), 4-diphenylphosphine oxide-4′,4″,4‴-tri(9H-carbazol-9-yl)-tetraphenylsilane (pTCSPO) and 4-diphenylphosphine oxide -4′-[3,6-di(9H-carbazol-9-yl)-9H-carbazol-9-yl]-tetraphenylsilane (TCSPO), containing different ratios and linking fashions of p-type carbazole units and n-type phosphine oxide units, are designed and obtained. DCSPO is the best host in FIrpic-doped devices for this series of compounds. By utilizing DCzSi and DPOSi as hole- and electron-transporting layers, a high EQE of 27.5% and a maximum current efficiency of 49.4 cd A^{-1} are achieved in the DCSPO/FIrpic doped device. Even at 10 000 cd m^{-2}, the efficiencies still remain 41.2 cd A^{-1} and 23.0%, respectively.

1. Introduction

Wide-bandgap materials that emit violet or ultraviolet (UV) light (emission shorter than 400 nm) are of great importance, since such devices can be used to generate light of all colors, either by energy transfer or by the irradiation of luminescent dyes.[1–3] Over the past decade, the development of organic wide-bandgap materials has been far behind their inorganic counterparts, which has resulted in a scarcity of UV organic light-emitting diodes (OLEDs) with high performance. One reason for this phenomenon is that it is difficult to simultaneously inject holes and electrons into wide-bandgap organic semiconductors because of their intrinsic, low highest occupied molecular orbital (HOMO) energy levels and high lowest unoccupied molecular orbital (LUMO) energy levels.[3,4] The restriction in the π-conjugation length results in the reduction of the carrier-injection and transport properties. Thus, it is quite challenging to design materials capable of giving efficient UV emission and that have balanced charge-injection properties.

High efficiency in OLEDs is a crucial factor in promoting their application. The host/phosphorescent-guest doping strategy is an important approach for this purpose. In doping systems, a wide-bandgap host material is a critical factor for high efficiency in blue OLEDs. In recent years, tetra-arylsilane derivatives have emerged as an attractive class of host material, due to their ultrahigh energy gap and high triplet energy level, and some of them have achieved a high quantum efficiency in host/blue-phosphorescent OLEDs. Typical materials are ultrawide energy gap hosts (UGHs),[4] tirphenyl-(4-(9-phenyl-9H-fluoren-9-yl)phenyl)silane (TPSi-F),[5] 4,4′-bis-triphenylsilanyl-biphenyl (BSB),[6] 4,4″-bis(triphenylsilanyl)-(1,1′,4′,1″)-terphenyl (BST),[6] $(9,9'\text{-dimethylfluoren-2-yl})_n\text{Si(phenyl)}_{4-n}$ (SiFln, n = 1, 2, 3, and 4),[7] 3,5-bis(9-carbazolyl)tetraphenylsilane (SimCP),[8] and 9-(4-tertbutylphenyl)-3,6-bis(triphenylsilyl)-9H-carbazole (CzSi).[9] Our group has also reported the substitution of tetraphenylsilane with carbazole, to obtain a high-triplet-energy host material, bis(4-(9-carbazolyl)phenyl)diphenylsilane (DPSiCBP),[10] which shows a higher quantum efficiency than 4,4′-bis(9-carbazolyl-)2,2′-biphenyl (CBP) in blue-phosphorescent OLEDs. The common character of the hosts mentioned above is that they predominantly transport holes. A problem still remains in terms of electron injection and transport. The phosphine oxide (PO) moiety is known to transport electrons predominantly as a point of saturation, since first reported by Sapochak's group.[11] The study has been intensified by several groups, to bond it with biphenyl,[11] fluorene,[12–14] carbazole,[15–19] spirobifluorene,[20] amine,[21,22] dibenzofuran,[23,24] and dibenzothiophene[19] moieties. The results show that the PO moiety can lower the LUMO level and increase the

Dr. H. Liu, Dr. D. H. Hu, Dr. F. Z. Shen, Dr. Y. Lv, G. N. Sun, Prof. B. Yang, Dr. P. Lu, Prof. Y. G. Ma
State Key Laboratory of Supramolecular Structure and Materials
Jilin University
Changchun, 130012, P. R. China
E-mail: lup@jlu.edu.cn; ygma@jlu.edu.cn
Dr. G. Cheng
State Key Laboratory on Integrated Optoelectronics
College of Electronics Science and Engineering
Jilin University
Changchun, 130012, P. R. China

DOI: 10.1002/adfm.201103126

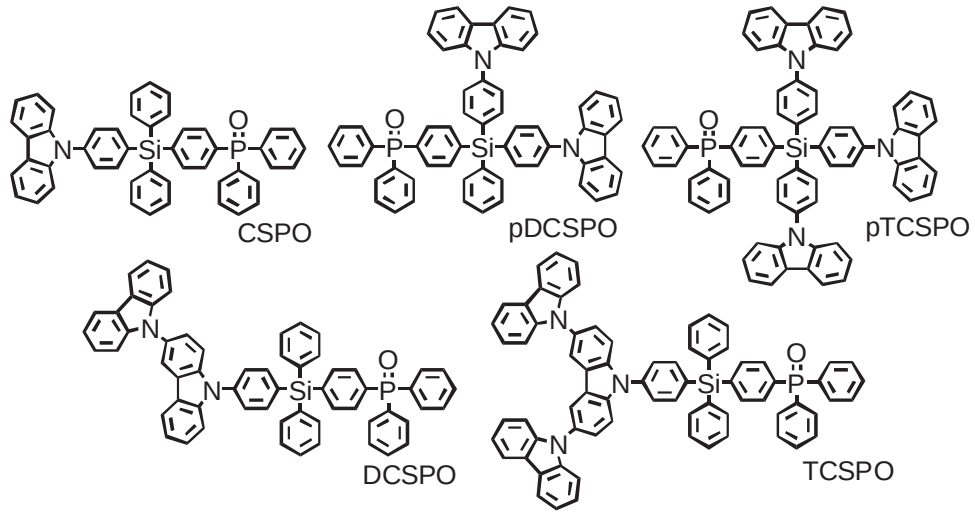

Scheme 1. Chemical structures of the five compounds.

electron-injection property without changing the triplet energy (E_T) of the molecule. Incorporating the PO moiety into carbazole-tetraphenylsilane to construct a bipolar-type wide-bandgap material would be interesting.

Lee's group reported one compound to connect PO with carbazole-substituted tetraphenylsilane (4-((4-(9H-carbazol-9-yl)phenyl) diphenylsilyl)phenyl)-diphenylphosphine oxide (TSPC) and an external quantum efficiency (EQE) of 21.8% was obtained when doping with iridium(III) bis[(5-cyano-4-fluorophenyl)pyridinato-$N,C^{2'}$]picolinate (FCNIrpic).[25] However, a systematic study of different ratios and various linking fashions of p-type and n-type units was not carried out. In this paper, we have developed five wide-bandgap materials: 4-diphenylphosphine oxide-4′-9H-carbazol-9-yl-tetraphenylsilane (CSPO), 4-diphenylphosphine oxide-4′,4″-di(9H-carbazol-9-yl)-tetraphenylsilane (pDCSPO), 4-diphenylphosphine oxide-4′-[3-(9H-carbazole-9-yl)-9H-carbazol-9-yl]-tetraphenylsilane (DCSPO), 4-diphenylphosphine oxide-4′,4″,4‴-tri(9H-carbazol-9-yl)-tetraphenylsilane (pTCSPO), and 4-diphenylphosphine oxide-4′-[(3,6-di(9H-carbazol-9-yl)-9H-carbazol-9-yl]-tetraphenylsilane (TCSPO), taking tetraphenylsilane as the core, functionalized with different ratios of p-type carbazole and n-type PO units, to pursue a balanced charge-injecting and -transporting ability. We found that a carbazole dimer coupled with a PO moiety in DCSPO is the best choice for this series of materials. A high current efficiency of 49.4 cd A^{-1} and an EQE of and 27.5%, with Commission Internationale de l'Eclairage (CIE) coordinates of (0.15, 0.28), was demonstrated by using DCSPO as host in bis[2-(4,6-difluorophenyl)pyridinato-C2,N](picolinato) iridium(III) (FIrpic)-doped OLEDs: this is the best efficiency value among the blue OLEDs reported in the literature.

2. Results and Discussion

2.1. Synthesis and Characterization

All of the compounds in this work had a tetraphenylsilane core (**Scheme 1**). The ratio of p-type carbazole and n-type PO units was designed as 1:1 for CSPO, 2:1 for pDCSPO, and 3:1 for pTCSPO. The carbazole was also designed to bond with the tetraphenylsilane, separately in pDCSPO and pTCSPO, or as dimers and trimers in DCSPO and TCSPO. All of these materials were synthesized through an Ullmann type reaction between the respective substituted carbazoles and phosphine oxide monomers. They were purified by column chromatography, followed by recrystallization from a mixture of dichloromethane and ethanol. The chemical structures were fully characterized by ^{1}H NMR and ^{13}C NMR spectroscopy, mass spectrometry, and elemental analysis, and they corresponded well with the expected structures.

2.2. Thermal Properties

High glass-transition temperatures (T_g) above 110 °C were observed for these materials (**Figure 1**). We found that the T_g rose gradually with the increasing number of carbazole units. The linking fashion also had an effect on the T_g. DCSPO and

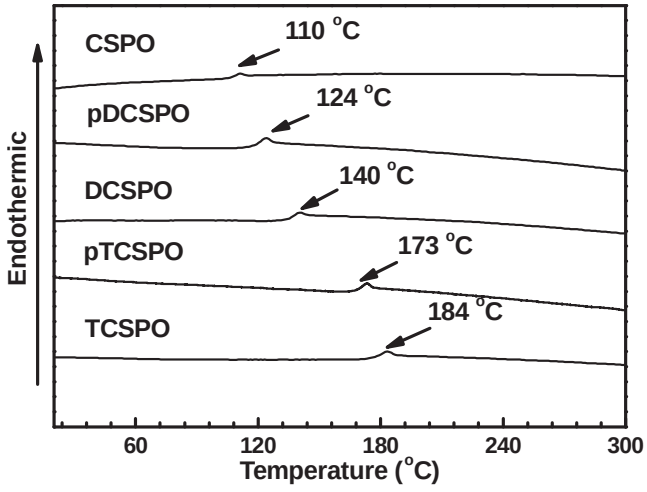

Figure 1. DSC data recorded at a heating rate of 10 K min^{-1}.

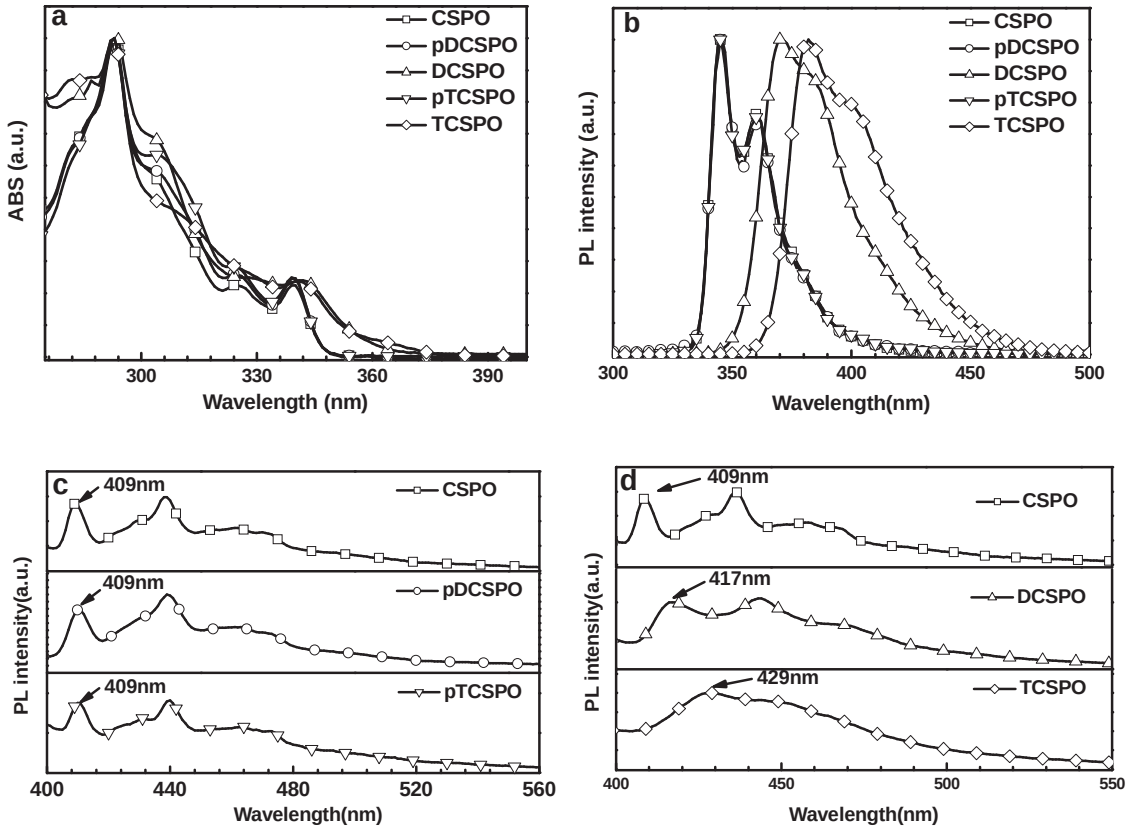

Figure 2. a,b) Absorption (a) and photoluminescence (PL) (b) spectra in THF solution at 10^{-5} M. c,d) PL at 77 K in frozen THF.

TCSPO both showed a T_g more than 10 °C higher than that of pDCSPO and pTCSPO, indicating dimer and trimer carbazole groups are more stable than those solely connected in pDCSPO and pTCSPO. They also exhibited a high thermal-decomposition temperature (T_d), ranging from 420 °C to 530 °C (Figure S1, Supporting Information). All of the five materials had better thermal properties than commonly used hosts, such as 1,3-bis(9-carbazolyl)benzene (mCP). The introduction of the carbazole and PO groups improved the thermal stability of the tetra-arylsilanes greatly, which is highly important for their application in devices.

2.3. Photophysical Properties

The different linking fashions led to different bandgaps and conjugation lengths for the molecules. For example, CSPO, pDCSPO, and pTCSPO showed the same absorption and emission spectra in tetrahydrofuran (THF) because of the same building fragments (**Figure 2**a). The maximum absorption peak at 293 nm and the absorption band from 324 nm to 344 nm are attributed to the π–π^* transition of the carbazole. As compared, DCSPO and TCSPO showed a red shift and a broadening band in the absorption spectrum, which was due to the enlarged conjugation through the substituted dimer and timer carbazole unit. The optical-energy band gaps (E_g), calculated from the onset of absorption, are 3.56 eV for CSPO, pDCSPO, and pTCSPO, and 3.38 eV for DCSPO and TCSPO. The emission spectra (Figure 2b) showed the same phenomena as the absorption spectra. The further red shift of the signal for the DCSPO and TCSPO indicates a larger conjugation. To evaluate the E_T of these materials, the emission at low temperature was also measured. The E_T ranged from 2.89 eV to 3.02 eV (Figure 2c,d), which is higher than that of FIrpic (E_T = 2.67 eV), indicating that the confinement of the triplet excitation on the dye was guaranteed. The photophysical data are summarized in **Table 1**.

2.4. Electrochemical Properties

Similar phenomena caused by the different linking fashions were also observed in the electrochemical properties during

Table 1. The photophysical and thermal properties.

	Abs_{max} [a)] [nm]	PL_{max} [a)] [nm]	E_g [a)] [eV]	E_T [b)] [eV]	T_g [c)] [°C]	T_d [d)] [°C]
CSPO	293, 325, 340	345, 360	3.56	3.02	110	420
pDCSPO	293, 325, 340	345, 361	3.56	3.02	124	433
DCSPO	293, 342	370	3.35	2.97	140	420
pTCSPO	293, 325, 340	345, 360	3.56	3.02	173	529
TCSPO	293, 342	382	3.38	2.89	184	512

[a)]Measured in THF solution at 10^{-5} M; [b)]Measured in frozen THF; [c)]Obtained from DSC measurements; [d)]Obtained from TGA measurements.

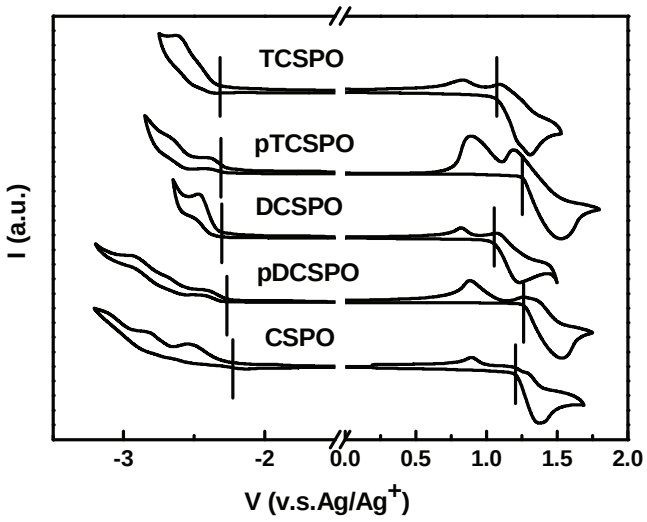

Figure 3. The CV curves in acetonitrile/CH_2Cl_2.

cyclic voltammetry (CV) measurements (**Figure 3**). In the cathodic scan, CSPO, pDCSPO, and pTCSPO underwent the same oxidation processes, originating from their p-type sole carbazole unit. Thus, they exhibited similar HOMO energy levels of about –5.60 eV. For the DCSPO and the TCSPO, the carbazole was designed as a dimer and a trimer, which made oxidation occur more easily, resulting in higher HOMO levels of about –5.43 eV, which is 0.17 eV higher than that of CSPO, pDCSPO, and pTCSPO. The LUMO levels of the five materials were identical, all being about –2.20 eV, caused by the same reduction PO unit. As compared, the LUMO energy level of pDCSPO was 0.2 eV lower than that of the compound we reported previously, DPSiCBP,[10] which had the same carbazole group, but was without the PO units. This result indicates that, on the one hand, PO can indeed lower the LUMO energy level; on the other hand, dimer and trimer carbazole groups can increase the HOMO energy level.

2.5. Theoretical Calculations

To understand the electronic properties further, density functional theory (DFT) calculations were carried out with the geometry optimized at the B3LYP/6-31G* level. The distributions of the front molecular orbital are shown in **Figure 4** and Figure S2 (Supporting Information); the HOMO and LUMO distributions

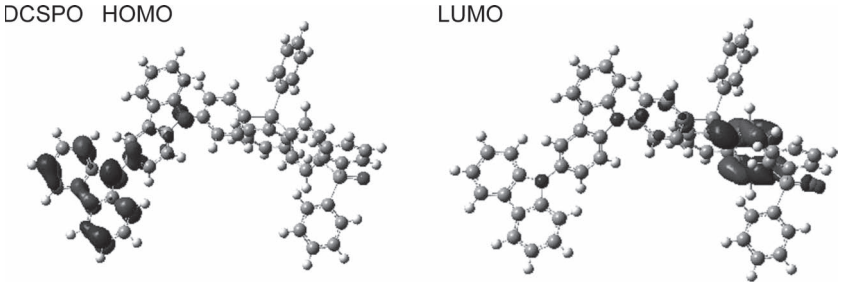

Figure 4. Simulation of front molecular orbital of DCSPO through DFT calculation.

Table 2. HOMO and LUMO energy level of the five materials.

	HOMO[a)] [eV]	LUMO[a)] [eV]	E_g[a)] [eV]	HOMO[b)] [eV]	LUMO[b)] [eV]	E_g[b)] [eV]
CSPO	–5.60	–2.25	3.35	–5.40	–1.05	4.35
pDCSPO	–5.59	–2.20	3.36	–5.39	–1.12	4.27
DCSPO	–5.43	–2.19	3.24	–5.16	–1.11	4.05
pTCSPO	–5.57	–2.20	3.37	–5.48	–1.17	4.31
TCSPO	–5.46	–2.20	3.26	–5.20	–1.22	3.98

[a)]Determined from the onset of the oxidation/reduction voltages; [b)]Calculated from the theoretical simulations.

of the CSPO, pDCSPO, DCSPO, and pTCSPO were completely separated, which resulted from the disruption effect of the tetraphenylsilane between the electron-rich and electron-deficient moieties. Taking DCSPO as an example (Figure 4), the HOMO level was located on the carbazole dimer units. The LUMO level was distributed on the benzene ring adjacent to the PO moiety. Interestingly, the HOMO level of TCSPO was the same as that of the other four materials. However, the LUMO+1 level, instead of the LUMO level, was distributed on the benzene ring close to PO group. The data are shown in **Table 2**.

2.6. Electroluminescence Properties

To evaluate the effects of the different ratios and linking fashions of the D-A group in the blue-phosphorescent OLEDs, doped FIrpic devices were evaluated. Devices A-E were fabricated with the structure of indium tin oxide (ITO)/poly(3,4-ethylenedioxythiophene):poly(styrenesulfonate) (PEDOT:PSS)/*N*,*N*′-di(1-naphthyl)-*N*,*N*,-diphenylbenzidine (NPB) (80 nm)/mCP (30 nm)/host:FIrpic (30 nm, 16 wt%)/1,3,5-tri(1-phenyl-1H-benzimidazol-2-yl)benzene (TPBI) (50 nm)/LiF (0.5 nm)/Al (100 nm). NPB and TPBi were used as hole- and electron-transporting layers, and mCP was used as an exciton-blocking layer. The energy levels of the correlative materials used in the devices are depicted in **Figure 5**a.

The differences of the ratios and linking fashions of the p-type and n-type units led to totally different device performances. As Lee reported a 21.8% EQE using CSPO as the host, we found that the 1:1 ratio of the carbazole and PO moiety for the host is not the best choice for blue OLEDs. Device C, hosted by DCSPO (carbazole dimer and PO moiety), showed the best performance. The maximum current efficiency and EQE could reach 24.6 cd A^{-1} and 11.2%, respectively (**Figure 6**). The EQE roll-off of device C was only 3.5% at 100 cd m^{-2} and 7.1% at 1000 cd m^{-2}. We think that the HOMO level of the DCSPO was about 0.2 eV higher than that of CSPO, which may have resulted in a more-balanced ratio of holes and electrons injected into the emissive layer and improved the device performance. The efficiency of device E (TCSPO) decreased a little, compared with device C, which means the carbazole dimer was the best couple for the PO unit.

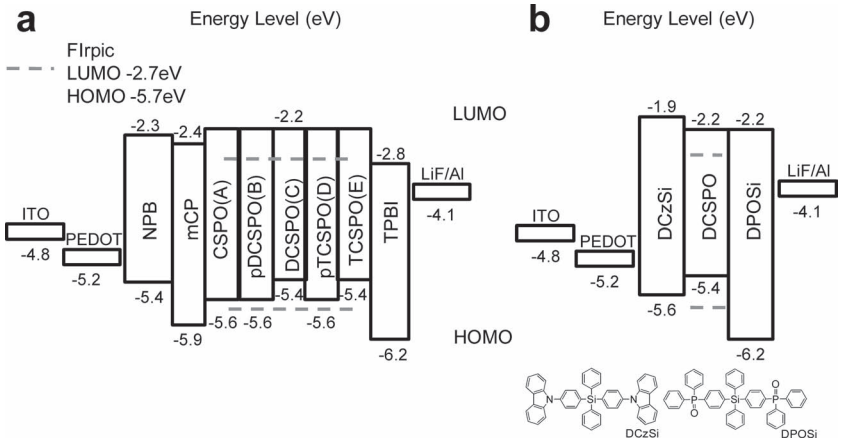

Figure 5. a) Energy-level diagrams for devices A–E. b) Energy-level diagram for device I and the structure of DCzSi and DPOSi.

Although the 2:1 ratio of the donor and acceptor in DCSPO showed a good device performance, pDCSPO, which also had the same 2:1 ratio of donor and acceptor but a different linking position, did not show satisfactory device performance. The *J*–*V* and efficiency curves illustrated that device B, hosted by pDCSPO, had a higher current density and a lower efficiency than device A, indicating that device B had unbalanced hole- and electron-injection and transport properties. Considering the structures of these two materials, we think the hole injection and transport of device B was much more than that of electrons. The further decrease of efficiency in device D (pTCSPO) demonstrates the same result as device B. The coupling of the carbazole dimer with PO would be the best choice for FIrpic for this series of materials. The data are listed in **Table 3**.

To optimize the performance of DCSPO in phosphorescent OLEDs further, we changed the hole and electron injection layers. We synthesized 4,4′-di(9H-carbazol-9-yl)-tetraphenylsilane (DCzSi) and 4,4′-bis(diphenylphosphine oxide)-tetraphenylsilane (DPOSi), to use them as hole- and electron-transporting layers, respectively. They had a similar chemical structure as the host (DCSPO) in the emissive layer (EL), indicating the better compatibility of hole-transporting layer (HTL), electron-transporting layer (ETL), and EL. Additionally, the large E_g (3.52 eV for DCzSi and 4.32 eV for DPOSi) and high E_T (3.02eV for DCzSi and 3.40 eV for DPOSi) could block nearly all of the excitons in the EL, which ensured the high efficiency of the device. Devices F–I, with structures of ITO/PEDOT:PSS/HTL(40 nm)/DCSPO:FIrpic (30 nm, 8 wt%)/ETL (30 nm)/LiF (0.8 nm)/Al (100 nm), were fabricated, and the details are shown in **Figure 7** and **Table 4**. Device F and H had a higher current density but a lower efficiency than those of devices G and I, indicating the carriers were confined well by applying DPOSi as the ETL. According to the energy diagram shown in Figure 5b, there was almost no injection barrier for holes

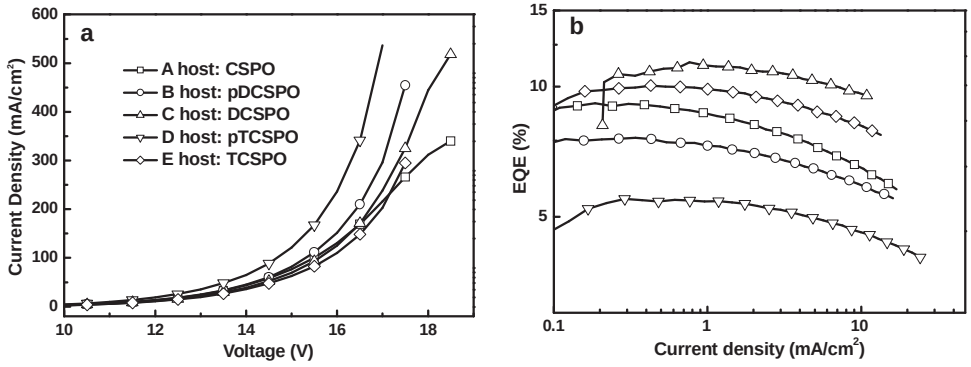

Figure 6. a) Current-density–voltage characteristics for devices A–E. b) Curves of external quantum efficiency versus current density for devices A–E.

Table 3. Device performance of devices A–E: V_{on} = turn - on voltage; brightness = maximum luminance; CE = current efficiency; PE = power efficiency; EQE = external quantum efficiency.

Device	V_{on} (V)	Brightness [cd m^{-2}]	CE_{max} [cd A^{-1}]	PE_{max} [lm W^{-1}]	EQE_{max} [%]	CE[a)] [cd A^{-1}]	PE[a)] [lm W^{-1}]	EQE[a)] [%]	CE[b)] [cd A^{-1}]	PE[b)] [lm W^{-1}]	EQE[b)] [%]
A	3.4	11 668	19.6	9.1	9.1	19.3	7.7	8.8	14.8	4.3	7.0
B	3.6	20 328	16.1	7.7	7.6	15.7	6.2	7.4	13.0	3.7	6.1
C	3.6	29 909	24.6	9.9	11.2	23.9	9.6	10.8	22.9	6.9	10.4
D	4.0	17 199	12.0	5.1	5.5	12.0	4.6	5.4	10.1	2.8	4.6
E	3.6	23 229	22.3	9.4	10.0	22.3	8.8	10.0	19.4	5.6	8.7

[a)]Value at 100 cd m^{-2}; [b)]Value at 1000 cd m^{-2}.

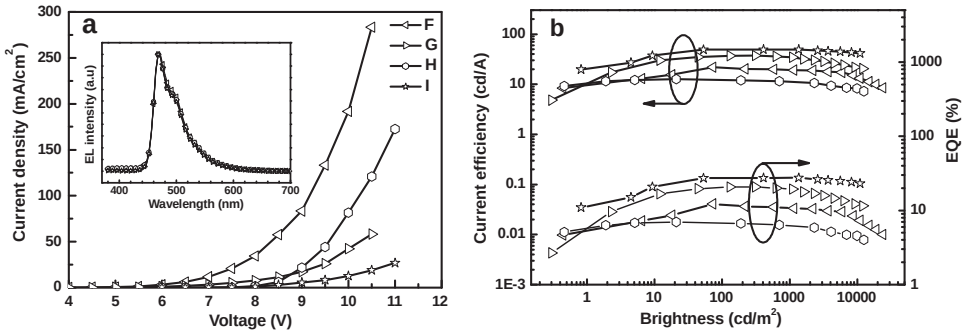

Figure 7. a) *J–V* curves for devices F–I. Inset: EL spectra of devices F–I at 8 V. b) Curves of current efficiency and EQE versus brightness for devices F–I.

Table 4. Details of devices F–I.

Device	HTL	ETL	V_{on} [V]	Brightness [cd m^{-2}]	CE_{max} [cd A^{-1}]	PE_{max} [lm W^{-1}]	CIE [*x*, *y*]
F	NPB (30 nm)/mCP (10 nm)	TPBi	3.5	24 000	21.9	13.8	0.15, 0.28
G	NPB (30 nm)/mCP (10 nm)	DPOSi	3.5	12 000	37.2	22.1	0.14, 0.28
H	DCzSi	TPBi	6.0	12 500	12.6	5.5	0.15, 0.28
I	DCzSi	DPOSi	6.0	11 000	49.4	20.5	0.15, 0.28

and electrons from the DCzSi and DPOSi to the EL in device I. The maximum current efficiency and EQE of device I reached 49.4 cd A^{-1} and 27.5%, respectively. Even at 10 000 cd m^{-2}, the current efficiency and EQE remained at 41.2 cd A^{-1} and 23.0%, respectively. Employing full wide-bandgap materials and a double blocking device structure are effective ways to obtain a high efficiency. This is the best device performance based on FIrpic.

3. Conclusions

In summary, we have designed different ratios and linking fashions of p-type carbazole and n-type PO moieties on tetraphenylsilane to pursue balanced charge injection and transport. The dimer and trimer carbazole-linking fashions could induce a longer conjugation length and increase the HOMO energy level. More balanced charge injection and transport was realized in DCSPO with dimer-carbazole/PO-substituted tetraphenylsilane. By applying DCzSi and DPOSi as an HTL and an ETL, respectively, the maximum current efficiency and EQE of devices based on DCSPO could reach 49.4 cd A^{-1} and 27.5%, respectively, with very low roll-off. The results indicate that PO and carbazole-substituted tetraphenylsilane can be utilized to construct wide-bandgap materials with good semiconducting properties.

4. Experimental Section

Measurements: The ^{1}H and ^{13}C NMR spectra were recorded using a Bruker AVANCE 500 spectrometer at 500 MHz and 125 MHz respectively, at 298 K using $CDCl_3$ as the solvent and tetramethylsilane (TMS) as the internal standard. UV–vis and fluorescence spectra were recorded using, respectively, a Shimadzu UV-3100 spectrophotometer and a Shimadzu RF-5301PC spectrophotometer, and using 1 cm-path-length quartz cells. DSC analysis was carried out using a NETZSCH (DSC-204) instrument at 10 K min^{-1} while flushing with nitrogen. Electrochemical measurements were performed using a BAS 100W Bioanalytical System: a glass-carbon disk electrode was used as the working electrode, a Pt wire as the counter electrode, Ag/Ag^+ as the reference electrode and Bu_4NPF_6 (0.1 M) in *N*,*N*-dimethylformamide (DMF) or CH_2Cl_2 as the electrolyte. The devices were fabricated by vacuum evaporation. The ITO-coated glass substrates were cleaned in an ultrasonic bath with toluene, acetone, ethanol, and deionized water, respectively; they were then dried with nitrogen and were finally irradiated in a UV-ozone chamber. The organic materials were sequentially deposited onto the cleaned ITO glass substrates through thermal evaporation. The layer thickness of the deposited material was monitored in situ using an oscillating-quartz thickness monitor. Finally a LiF buffer layer and an Al cathode were deposited onto the organic films. The background pressure of the chamber was less than 10^{-6} Torr during the deposition process. The luminance–current characteristics of devices A to E were measured using a PR650 spectroscan spectrometer and those of devices F to I were measured using a PR655 spectroscan spectrometer. The current–voltage characteristics were studied using a Keithley 2400 sourcemeter. All of the device measurements were carried out at room temperature under ambient conditions. The EQE was calculated according to a method reported previously by Okamoto et al.[26]

Synthesis of 4-Diphenylphosphine oxide-4′-9H-carbazol-9-yl-tetraphenylsilane (CSPO): A mixture of 4-bromo-4′-diphenylphosphine oxide-tetraphenylsilane (1.23 g, 2.00 mmol), carbazole (368 mg, 2.20 mmol), CuI (38 mg, 0.20 mmol), K_3PO_4 (1.06 g, 5.00 mmol), and (±)-*trans*-1,2-diamino-cyclohexane (280 mg, 0.20 mmol) was added to 1,4-dioxane (5 ml), then refluxed under nitrogen for 24 h. After cooling, the reaction mixture was quenched with $(NH_4)_2CO_3$ solution and extracted with CH_2Cl_2, then dried over anhydrous $MgSO_4$. After removal of the solvent, the residue was purified by column chromatography on silica gel using ethyl acetate/petroleum (1:2 v/v) as the eluent, followed by recrystallizing with CH_2Cl_2 and ethanol to give a white powder. Yield: 60%; ^{1}H NMR (500 MHz, $CDCl_3$, δ): 7.287–7.316 (2H, t, J = 7.324, Ar H), 7.402–7.513 (14H, m, Ar H), 7.547–7.577 (2H, t, J = 7.324, Ar H), 7.613–7.640 (6H, t, J = 6.104, J = 7.324), 7.689–7.793 (10H, m, Ar H), 8.13–8.159 (2H, d, J = 7.629, Ar H); ^{13}C NMR (125 MHz, $CDCl_3$, δ): 140.55, 139.33, 137.90, 134.45, 133.63, 133.00 132.60, 132.20, 132.13, 131.77, 131.36, 131.30, 130.16, 128.65, 128.56, 128.23, 126.28, 126.00, 123.59, 120.37, 120.18, 109.90; MALDI-TOF-MS (M) (*m*/*z*): 703.2 $[M + H]^+$; Anal. calcd for $C_{48}H_{36}NOPSi$: C 82.14, H 5.17, N 2.00; found: C 81.99, H 5.27, N 2.00.

Synthesis of 4-Diphenylphosphine oxide-4′,4″-di(9H-carbazol-9-yl)-tetraphenylsilane (pDCSPO): pDCSPO was prepared according to a similar procedure to CSPO using 4,4′-dibromo-4″-diphenylphosphine oxide-tetraphenylsilane to replace the 4-bromo-4′-diphenylphosphine oxide-tetraphenylsilane. Yield: 70%; ^{1}H NMR (500 MHz, $CDCl_3$, δ):

8.162–8.147 (4H, d, J = 7.935, Ar H), 7.874–7.825 (5H, m, Ar H), 7.789–7.675 (12H, m, Ar H), 7.583–7.469 (14H, m, Ar H), 7.439–7.408 (4H, t, J = 7.019, J = 8.240, Ar H), 7.321–7.291 (4H, t, J = 7.324, J = 7.629, Ar H); ^{13}C NMR (125 MHz, $CDCl_3$, δ): 140.54, 139.58, 138.99, 137.95, 136.45, 134.76, 133.94, 132.70, 132.16, 131.71, 131.52, 131.46, 130.40, 128.70, 128.61, 128.42, 126.43, 126.05, 123.64, 120.42, 120.27, 109.91; MALDI-TOF-MS (M) (m/z): 868.8 $[M + H]^+$; Anal. calcd for $C_{60}H_{43}N_2OPSi$: C 83.11, H 5.00, N 3.23; found: C 81.89, H 5.10, N 3.26.

Synthesis of 4-Diphenylphosphine oxide-4′-[3-(9H-carbazole-9-yl)-9H-carbazole-9-yl]-tetraphenylsilane (DCSPO): DCSPO was prepared according to a similar procedure to CSPO using 3-(9H-carbazol-9-yl)-9H-carbazole to replace carbazole. Yield: 55%; ^{1}H NMR (500 MHz, $CDCl_3$, δ): 8.287–8.283 (1H, s, Ar H), 8.195–8.179 (2H, d, J = 8.240, Ar H), 8.120–8.105 (1H, d, J = 7.629, Ar H), 7.845–7.828 (2H, d, J = 8.240, Ar H), 7.781–7.639 (15H, m, Ar H), 7.577–7.387 (19H, m, Ar H), 7.340–7.283(3H, m, Ar H); ^{13}C NMR (125 MHz, $CDCl_3$, δ): 141.88, 141.28, 139.69, 139.24, 139.04, 138.09, 136.43, 134.52, 133.70, 133.25, 132.91, 132.57, 132.15, 131.74, 131.40, 131.35. 130.23, 130.13, 128.67, 12859, 128.28, 126.76, 126.35, 125.91, 125.56, 124.63, 123.17, 120.65, 120.33, 119.67, 119.54; MALDI-TOF-MS (M) (m/z): 868.6 $[M + H]^+$; Anal. calcd for $C_{60}H_{43}N_2OPSi$: C 83.11, H 5.00, N 3.23; found: C 81.48, H 5.07, N 3.26.

Synthesis of 4-Diphenylphosphine oxide-4′,4″,4‴-tri(9H-carbazol-9-yl)-tetraphenylsilane (pTCSPO): pTCSPO was prepared according to a similar procedure to CSPO using 4,4′,4″-dibromo-4‴-diphenylphosphine oxide-tetraphenylsilane to replace 4-bromo-4′-diphenylphosphine oxide-tetraphenylsilane. Yield: 63%; ^{1}H NMR (500 MHz, $CDCl_3$, δ): 8.173–8.157 (6H, d, J = 7.629, Ar H), 7.959–7.914 (8H, m, Ar H), 7.853–7.813 (2H, m, Ar H), 7.782–7.719 (10H, m, Ar H), 7.593–7.478 (12H, m, Ar H), 7.452–7.421 (6H, t, J = 7.324, J = 7.825, Ar H), 7.331–7.301 (6H, t, J = 7.324, J = 7.935, Ar H); ^{13}C NMR (125 MHz, $CDCl_3$, δ): 140.92, 140.22, 139.01, 138.39, 136.88, 136.81, 135.61, 134.82, 133.03, 132.59, 132.25, 132.08, 132.03, 129.13, 129.05, 126.98, 126.49, 124.10, 120.86, 120.75; MALDI-TOF-MS (M) (m/z): 1033.8 $[M + H]^+$; Anal. calcd for $C_{72}H_{50}N_3OPSi$: C 83.79, H 4.88, N 4.07; found: C 82.54, H 4.93, N 3.99.

Synthesis of 4-Diphenylphosphine oxide-4′-[(3,6-di(9H-carbazol-9-yl)-9H-carbazol-9-yl]-tetraphenylsilane (TCSPO): TCSPO was prepared according to a similar procedure to CSPO using 3,6-di(9H-carbazol-9-yl)-9H-carbazole to replace carbazole. Yield: 58%; ^{1}H NMR (500 MHz, $CDCl_3$, δ): 8.280–8.276 (2H, s, Ar H), 8.171–8.155 (4H, d, J = 7.324, Ar H), 7.902–7.885 (2H, d, J = 8.240, Ar H), 7.798–7.704 (12H, m, Ar H), 7.669–7.653 (4H, d, J = 7.935, Ar H), 7.629–7.607 (2H, d, J = 8.850, Ar H), 7.580–7.455 (12H, m, Ar H), 7.418–7.380 (8H, m, Ar H), 7.298–7.272 (4H, m, Ar H); ^{13}C NMR (125 MHz, $CDCl_3$, δ): 140.79, 139.58, 139.13, 138.67, 136.84, 134.29, 133.20, 132.88, 132.63, 132.56, 132.04, 131.86, 13178, 131.03, 130.69, 129.09, 129.00, 128.72, 126.82, 126.72, 126.35, 124.62, 123.62, 120.75, 120.17, 111.88, 110.12; MALDI-TOF-MS (M) (m/z): 1033.8 $[M + H]^+$; Anal. calcd for $C_{72}H_{50}N_3OPSi$: C 83.78, H 4.88, N 4.07; found: C 82.62, H 5.07, N 3.99.

Supporting Information

Supporting Information is available from the Wiley Online Library or from the author.

Acknowledgements

The authors are grateful for the support from the National Science Foundation of China (Grant No. 20834006, 21174050), the Ministry of Education of China (Grant No. 20070183202), the Ministry of Science and Technology of China (Grant No. 2009CB623605), and PCSIRT.

Received: December 23, 2011
Published online: April 13, 2012

[1] S. Nakamura, M. Senoh, S. Nagahama, N. Iwasa, T. Yamada, T. Matsushita, Y. Sugimoto, H. Kiyoku, *Appl. Phys. Lett.* **1996**, *69*, 4054058.
[2] H. Jia, L. Guo, W. Wang, H. Chen, *Adv. Mater.* **2009**, *21*, 4641.
[3] R. J. Holmes, B. W. D'Andrade, S. R. Forrest, X. Ren, J. Li, M. E. Thompson, *Appl. Phys. Lett.* **2003**, *83*, 3818.
[4] X. Ren, J. Li, R. J. Holmes, P. I. Djurovich, S. R. Forrest, M. E. Thompson, *Chem. Mater.* **2004**, *16*, 4743.
[5] P. Shih, C.-H. Chien, C.-Y. Chuang, C.-F. Shu, C.-H. Yang, J.-H. Chen, Y. Chi, *J. Mater. Chem.* **2007**, *17*, 1692.
[6] J.-J. Lin, W.-S. Liao, H.-J. Huang, F.-I. Wu, C.-H. Cheng, *Adv. Funct. Mater.* **2008**, *18*, 485.
[7] W. Wei, P. I. Djurovich, M. E. Thompson, *Chem. Mater.* **2010**, *22*, 1724.
[8] S.-J. Yeh, M.-F. Wu, C.-T. Chen, Y.-H. Song, Y. Chi, M.-H. Ho, S.-F. Hsu, C. H. Chen, *Adv. Mater.* **2005**, *17*, 285.
[9] M.-H. Tsai, H.-W. Lin, H.-C. Su, T.-H. Ke, C.-C. Wu, F.-C. Fang, Y.-L. Liao, K.-T. Wong, C.-I Wu, *Adv. Mater.* **2006**, *18*, 1216.
[10] D. Hu, P. Lu, C. Wang, H. Liu, H. Wang, Z. Wang, T. Fei, X. Gu, Y. Ma, *J. Mater. Chem.* **2009**, *19*, 6143.
[11] P. E. Burrows, A. B. Padmaperuma, L. S. Sapochak, P. Djurovich, M. E. Thompson, *Appl. Phys. Lett.* **2006**, *88*, 183503.
[12] A. B. Padmaperuma, L. S. Sapochak, P. E. Burrows, *Chem. Mater.* **2006**, *18*, 2389.
[13] F.-M. Hsu, C.-H. Chien, P.-I Shih, C.-F. Shu, *Chem. Mater.* **2009**, *21*, 1017.
[14] F.-M. Hsu, C.-H. Chien, C.-F. Shu, C.-H. Lai, C.-C. Hsieh, K.-W. Wang, P.-T. Chou, *Adv. Funct. Mater.* **2009**, *19*, 1.
[15] L. S. Sapochak, A. B. Padmaperuma, X. Cai, J. L. Male, P. E. Burrows, *J. Phys. Chem. C* **2008**, *112*, 7989.
[16] S. O. Jeon, K. S. Yook, C. W. Joo, J. Y. Lee, *Adv. Funct. Mater.* **2009**, *19*, 3644.
[17] J. Ding, Q. Wang, L. Zhao, D. Ma, L. Wang, X. Jing, F. Wang, *J. Mater. Chem.* **2010**, *20*, 8126.
[18] H.-H. Chou, C.-H. Cheng, *Adv. Mater.* **2010**, *22*, 2468.
[19] X. Cai, A. B. Padmaperuma, L. S. Sapochak, P. A. Vecchi, P. E. Burrows, *Appl. Phys. Lett.* **2008**, *92*, 083308.
[20] S. E. Jang, K. S. Yook, J. Y. Lee, *Org. Electron.* **2010**, *11*, 1154.
[21] E. Polikarpov, J. S. Swensen, N. Chopra, F. So, A. B. Padmaperuma, *Appl. Phys. Lett.* **2009**, *94*, 223304.
[22] J. S. Swensen, E. Polikarpov, A. V. Ruden, L. Wang, L. S. Sapochak, A. B. Padmaperuma, *Adv. Funct. Mater.* **2011**, *21*, 3250.
[23] P. A. Vecchi, A. B. Padmaperuma, H. Qiao, L. S. Sapochak, P. E. Burrows, *Org. Lett.* **2006**, *8*, 4211.
[24] C. Han, G. Xie, H. Xu, Z. Zhang, L. Xie, Y. Zhao, S. Liu, W. Huang, *Adv. Mater.* **2011**, *23*, 2491.
[25] Y. J. Cho, J. Y. Lee, *J. Phys. Chem. C.* **2011**, *115*, 10272.
[26] S. Okamoto, K. Tanaka, Y. Izumi, H. Adachi, T. Yamiji, T. Suzuki, *Jpn. J. Appl. Phys.* **2001**, *40*, 783.